Fabrication and Mechanical Properties of Al_2O_3-SiC/TiC/Ni Functionally Graded Materials by SHS/HIP †

Youping REN*, Junshan LIN, Yoshinari MIYAMOTO***, Guanjun QIAO**** and Zhihao JIN*******

Abstract

Dense Functionally Graded Materials (FGMs) in the systems of Al_2O_3/TiC/Ni and Al_2O_3-SiC/TiC/Ni were fabricated by SHS/HIP. Due to the rapid high temperature heating and the use of effective additives, the grain growth could be well controlled. The residual stress produced in the outer Al_2O_3 and Al_2O_3-SiC layers, which was induced by the thermal expansion mismatch between the inner TiC/Ni and the outer ceramic layers, was in the range of –220 MPa to –500 MPa. Two methods were used to measure the R-curve behavior of FGMs. For the indentation-strength method, the compressive stress of the outer ceramic layers showed steep R-curve behavior. For the single edge notch bend (SENB) method, the toughness of the FGM increased in the compression area and reached its maximum of 33MPam$^{1/2}$at the interface of the compressive stress and the tensile stress areas. In the tension area the value of toughness decreased.

KEY WORDS: (FGM;Functionally graded materials) (Al_2O_3/TiC/Ni) (Al_2O_3-SiC/TiC/Ni) (SHS/HIP) (R-curve behavior) (Toughness) (Residual stress)

1. Introduction

The residual stress in a material can be induced by anisotropy or mismatch of thermal expansion or phase transformation. The magnitude and the state of residual stress in ceramics has a vital effect on mechanical properties such as fracture stress, fracture toughness and wear resistance[1-3]. Generally it is tailored to obtain high surface compression with a moderate bulk tension. The introduction of this concept can be traced back to the work of H. P. Kirchner[4] in 1979. Some methods have been employed to produce surface compression, including heat treatments such as quenching, application of low expansion coatings, chemical modification of surfaces, and pressure induced phase transformation[5].

Various symmetric graded materials such as TiC/Ni/TiC[6] and Al_2O_3/TiC/Ni[7] have been fabricated. The results show that it is easy to tailor deep compressive layers by using layered or graded structures which are preferable for restraining the initiation or growth of microcracks. This concept is applied to cutting tools[8].

In the present study, symmetric FGMs in the system of Al_2O_3-SiC/TiC/Ni were fabricated by SHS/HIP and their mechanical properties such as strength, apparent fracture toughness and R-curve behavior were investigated. The SHS/HIP is a powerful and energy saving process to sinter FGMs[9].

2. Experimental Procedure

The starting materials used were Al_2O_3, TiC, Ni, SiC powders with an average particle size of 0.4μm, 1.4μm, 1.0μm, and 1.0μm, respectively. These powders were wet-mixed in pre-determined compositions for over 48 hours by ball milling, and then dried in a vacuum oven. Each sample was designed to have a symmetric five-layer structure. The compositions of each layer are shown in **Fig. 1**. The green body was press-formed at 200MPa by CIP and put into a glass capsule and vacuum sealed at 820°C. The sample was covered with BN powder bed in the capsule. Then, the glass encapsulated samples were put into the chemical oven including silicon powders of 40g which is charged in a graphite container. Two pieces of small ignition pellets consisting of Al and Fe_2O_3 powder mixtures were placed at just below and over the capsule in a chemical oven. The samples were sintered in

† Received on January 31, 2000
* Graduate Student, Xi'an Jiaotong University
** Post Doctoral Research Fellow
*** Professor
**** Associate Professor, Xi'an Jiaotong University
***** Professor, Xi'an Jiaotong University

Transactions of JWRI is published by Joining and Welding Research Institute of Osaka University, Ibaraki, Osaka 567-0047, Japan.

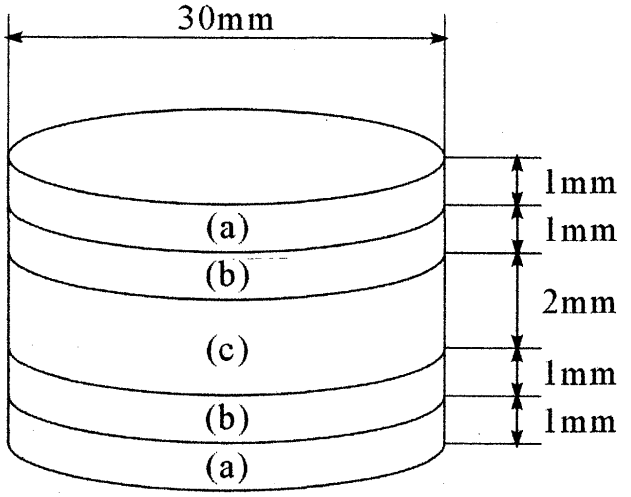

(a) Al_2O_3, Al_2O_3+10, 15, 20 vol.%SiC
(b) Al_2O_3+46.8vol.%TiC+2.5vol.%Ni
(c) TiC+19.8vol.%Ni+6.5vol.%Mo_2C

Fig. 1 Structure and composition of sintered FGM bodies.

the HIP equipment. All samples were fabricated at the HIP temperature of 1150°C for 30mins under a nitrogen gas pressure of 100MPa. In the course of heating up, the combustion reaction of silicon and nitrogen was induced by the exothermic reaction of thermite pellets at about 1050°C, so that the temperature in the chemical oven could reach as high as 2500°C for a few minutes due to the reaction heat, resulting in rapid densification. The glass capsule was melt, but not flew down and the sample was sintered without reaction with the glass capsule due to the protection of BN powder bed.

The sintered samples were disks of 30mm diameter and 6 ~ 7 mm thickness. They were polished to a diamond surface finish of 3μm. The compressive stress at the surface of FGMs was determined by the $\sin^2\psi$-2θ method using an X-ray diffraction peak (416) of Al_2O_3. Hardness and indentation toughness were measured by using a Vickers hardness-testing machine with an indentation load of 98N for 10 seconds. The indentation-induced crack length, 2C, was measured using an optical microscope and the indentation toughness, K_c, was calculated using the following equation[10]:

$$(K_c\phi / H_v a^{1/2}) / (H_v / E\phi)^{2/5} = 0.129(c/a)^{-3/2} \quad (1)$$

where ϕ is a material-independent constant. H_v, E, and a are Vickers hardness, Young's modulus and half-diagonal length of the indentation, respectively.

The sintered samples were cut into rectangular bar specimens with the size of 2x6x25 mm^3. The surfaces of a specimen were ground and the edges were slightly chamfered. The tensile face was polished to a 1μm finish. Flexural strength was measured by means of three-point bending test with a span length of 18 mm and cross head speed of 0.5 $mm \cdot min^{-1}$ using an Instron 1185 machine. The indentation-strength method was used to evaluate the R-curve behavior of FGMs[11,12]. The indentations with loads from 9.8 to 196N were applied at the center of the tensile face of a sample beam, and subsequently fractured by three-point bending. The indentation strength, crack length and load in bending experiments were used to calculated the R-curve: $K_R=k(\Delta c)^m$, where K_R is the fracture resistance, Δc is crack extension, and k, m are material constants. In addition, the toughness of FGMs according to the SEBN method was investigated. A diamond blade of 100μm thickness was used to introduce a notch into the sample. The toughness was calculated referring to ASTM Standard E-399[13]. The fracture surface was observed by scanning electron microscopy (SEM).

3. Results and Discussion

Figure 2 gives the fracture surface image of different FGMs. The photos (a), (b) and (c) show the surface layers of the Al_2O_3, the Al_2O_3-10v.%SiC, and Al_2O_3-15v.%SiC. Photo (d), (e), (f), and (g) show the interfacial regions of the first/second layer, second layer, interfacial region of the second/central layers, and central layer of the Al_2O_3/TiC/Ni system, respectively. Because the temperature as high as 2500°C is maintained only for several minutes, the grain growth is not severe. Also because the SiC particles can refine the microstructure, the grain size of the Al_2O_3-15v.%SiC layer was controlled to be smaller than that of the simple Al_2O_3 layer.

The mechanical properties of different FGMs and monolithic Al_2O_3 are summarized in **Table 1**. The compressive residual stress at the surface layers of FGMs rises with the increasing of the SiC content. The reason is that the addition of SiC with a lower thermal expansion coefficient than Al_2O_3 increases the thermal expansion mismatch between the outer and inner layers. The toughness and strength of the outer layer could be effectively enhanced due to the residual compressive stress. In the case of the Al_2O_3-20v.%SiC FGM, however, the sample was cracked when cutting due to a large tensile stress produced in the central layer.

Figure 3 shows indents introduced in the surfaces of two different FGMs and monolithic Al_2O_3. The effect of compressive residual stresses can be seen in the crack length for an indentation load of 10kg (98N); each crack length in the Al_2O_3 FGM, Al_2O_3-10v.%SiC FGM, Al_2O_3-15v.%SiC FGM, Al_2O_3-20v.%SiC FGM and the monoli-

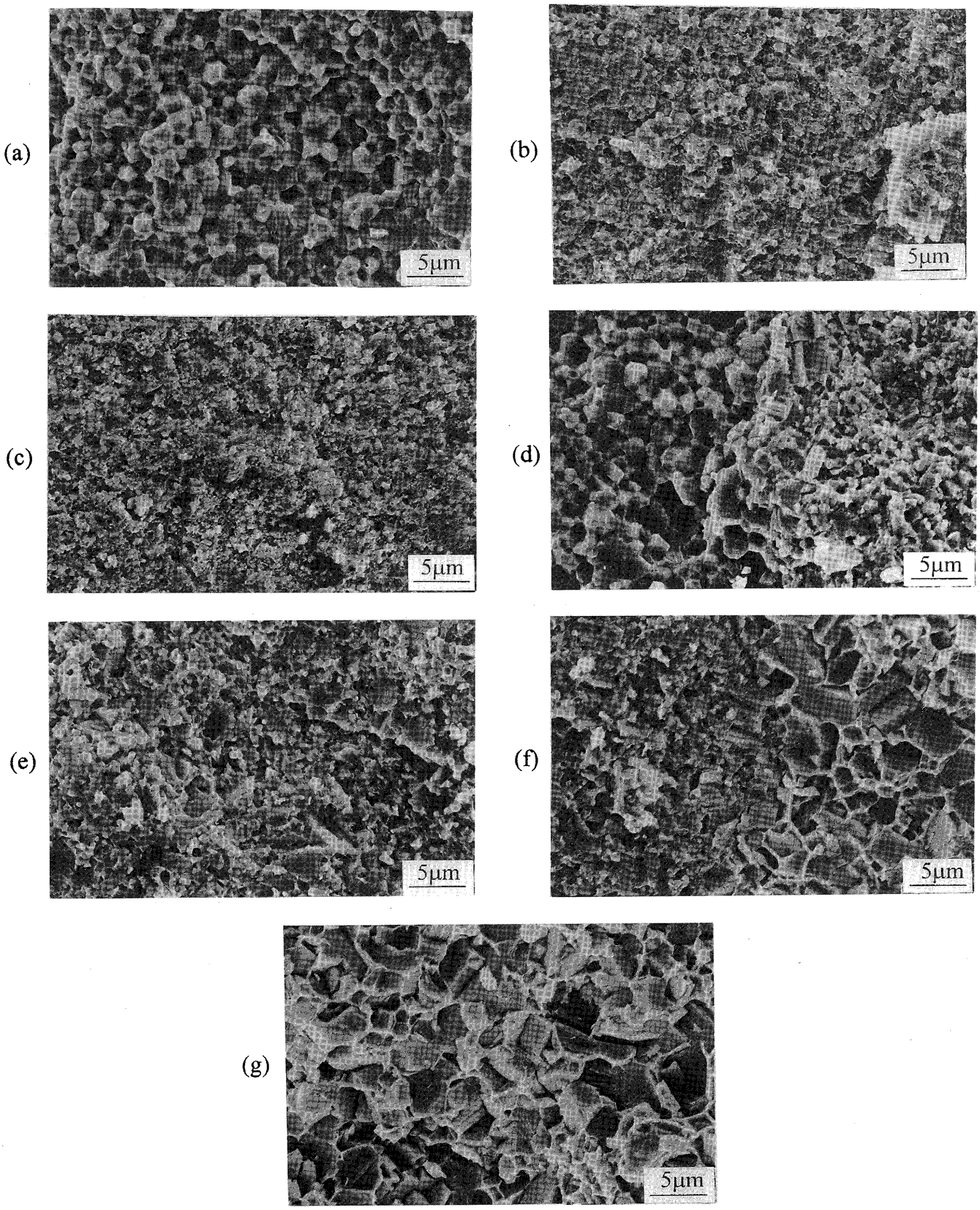

Fig. 2 SEM images of the fracture surfaces; (a) Outer Al_2O_3 layer, (b) Outer Al_2O_3-10v.%SiC layer, (c) Outer Al_2O_3-15v.%SiC layer, (d) Interfacial region of Al_2O_3/ Al_2O_3-TiC layer, (e) Al_2O_3-TiC layer, (f) Interfacial region of Al_2O_3-TiC/TiC-Ni layer, (g) Center TiC-Ni layer.

Table 1 Mechanical properties of FGMs and a monolithic Al_2O_3.

Properties / Materials	Hv(GPa)(10Kg)	K_{IC}(MPa·m$^{1/2}$) (10Kg)	Compressive stress (MPa) (by X-ray)	Strength(MPa)
Al_2O_3	18	4.0	0	400
Al_2O_3 FGM	20	6.0	-220	900
Al_2O_3-10vol%SiC FGM	21	6.9	-340	940
Al_2O_3-15vol%SiC FGM	21.5	7.5	-500	900
Al_2O_3-20vol%SiC FGM	22	7.71	-500	-

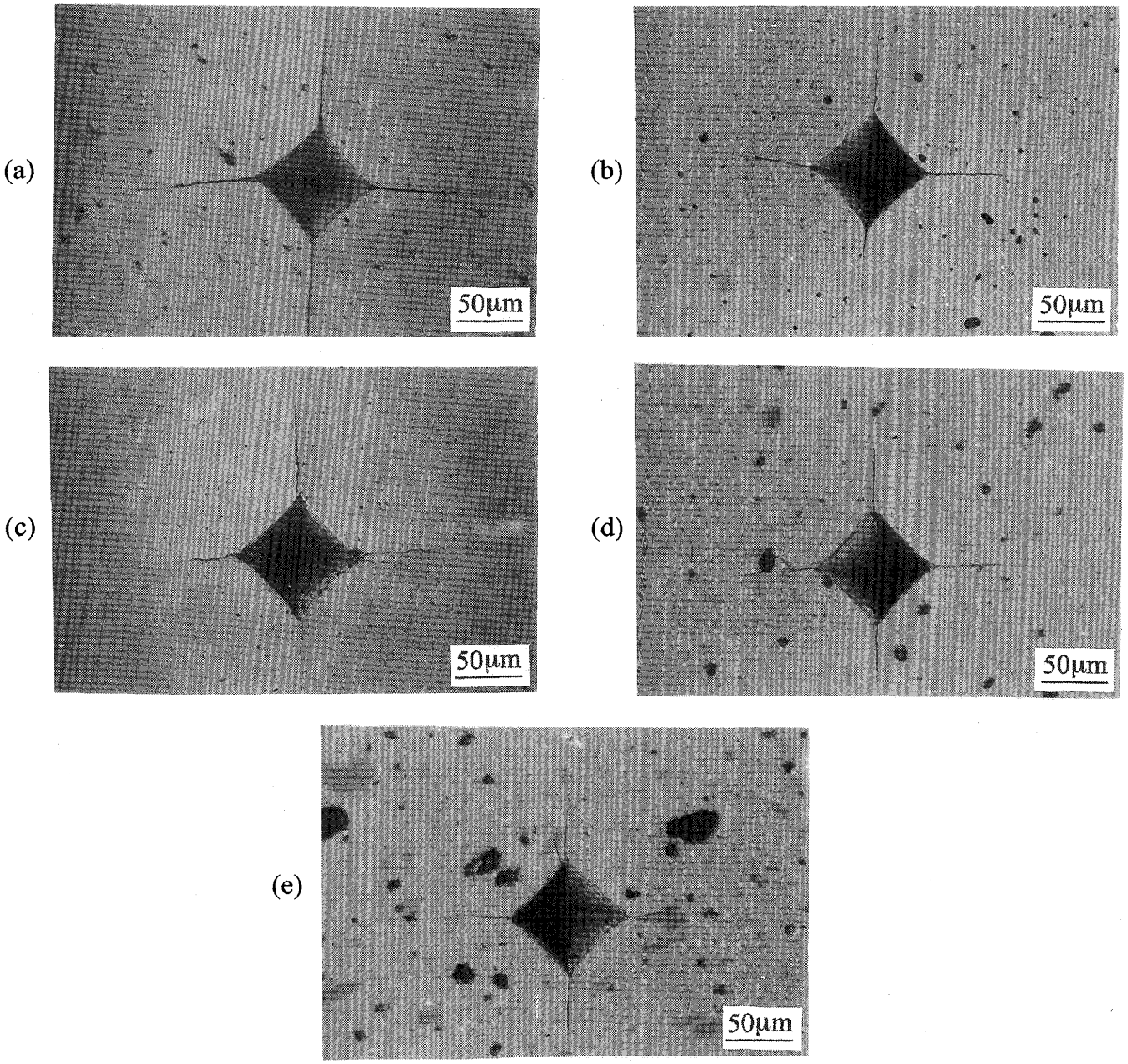

Fig. 3 Optical micrographs of indented samples: (a) monolithic Al_2O_3, (b) Al_2O_3 FGM, (c) Al_2O_3-10v.%SiC FGM, (d) Al_2O_3-15v.%SiC FGM, (e) Al_2O_3-20v.%SiC FGM.

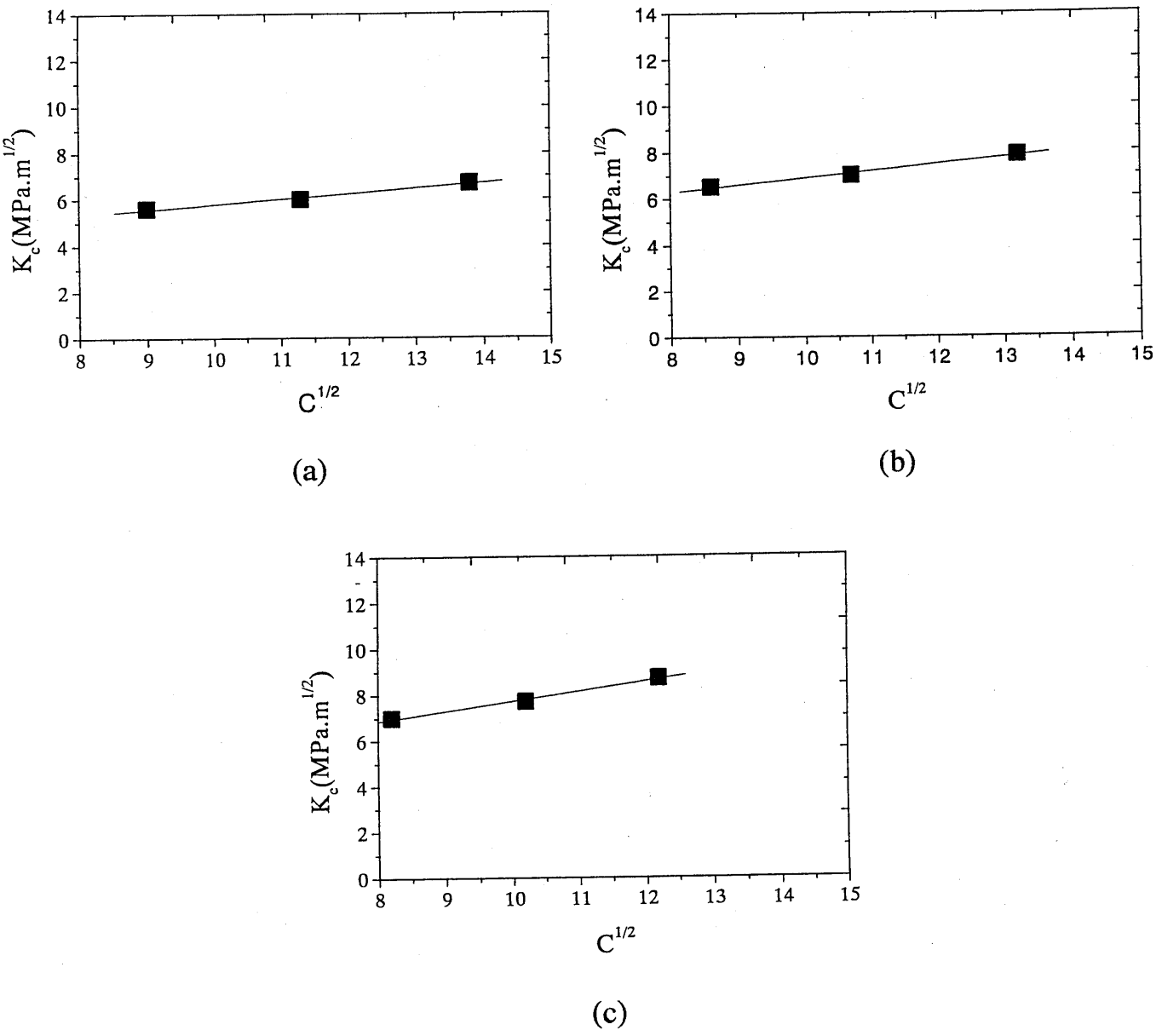

Fig. 4 Indentation toughness vs crack length (a) Al_2O_3 FGM, (b) Al_2O_3-10v.%SiC FGM, (c) Al_2O_3-15v.%SiC FGM.

thic Al_2O_3 extends to 127μm, 115μm, 105μm, 100μm, and 160μm, respectively.

The residual stress can be determined according to the indentation fracture mechanics for a half penny flaw. The indentation toughness, K_c, and the crack length can be related by the following equation[14]:

$$K_c = K_c^0 - 2\sigma_R(C/\pi)^{1/2} \quad (2)$$

where K_c^0 is the toughness of a ceramic without stress, σ_R is the residual stress in a ceramic and C is the indentation crack length. K_c^0 and σ_R can be obtained by linear fitting associated with K_c and $C^{1/2}$. **Figure 4** shows the plots of K_c versus $C^{1/2}$ of the three FGMs. The indentation loads are 49N, 98N, and 196N. For the Al_2O_3/TiC/Ni, the Al_2O_3-10v.%SiC/TiC/Ni FGMs, and the Al_2O_3-15v.%SiC/TiC/Ni FGM, the apparent fracture toughness rose with the increase of crack length. The calculated values for σ_R are listed in **Table 2**. Both values showed good coincidences.

Table 2 Comparison of calculated and measured residual stress (σ_R).

Materials	σ_R(MPa) Calculated	σ_R(MPa) Measured
Al_2O_3 FGM	-190	-220
Al_2O_3-10v.%SiC FGM	-260	-340
Al_2O_3-15v.%SiC FGM	- 370	-500

R-curve behavior arises because additional energy is consumed in the process zone of a propagating crack besides the fracture energy dissipated at the crack tip. The shape of an R-curve reflects the ability of ceramic to tolerate the crack extension and thus the strength reliability. It is very important, therefore, to characterize and understand the R-curve behavior of ceramics as well as the development of materials having an appropriate R-curve behavior. It has been manifested that the surface compressive stress can introduce a steep R-curve in a ceramic by a three-dimensional finite element analysis[15]. In this study, the compressive stress was induced by the thermal expansion mismatch between the outer and inner layers. Due to the addition of about 20v.% nickel whose thermal expansion coefficient is as high as 16×10^{-6}/°C, an apparent difference in thermal expansion coefficient of 1 ~ 2×10^{-6}/°C exists between the central and outer layers of the Al_2O_3/TiC/Ni FGMs, which causes a strong compressive stress of -220 ~ -300MPa in the outer layers. The central layer of TiC/Ni has a tensile stress of 300 ~ 400 MPa, which can be withstood because of the high strength of about 1000MPa.

The fracture resistance K_R, and the crack extension length, Δc, satisfies the following relationship[11]:

$$K_R=k(\Delta c)^m \quad (3)$$

where k is a constant and m is a characteristic exponent that describes the sensitivity of R-curve behavior. When m is zero, K_R is invariant with the crack extension. The exponent m can be obtained from the slope β of a log-log plot of post-indentation strength, S, versus indentation load, P.

$$m=(1-3\beta)/(2+2\beta) \quad (4)$$

$$k=Y\alpha(\beta\gamma)^{-\beta}(1+\beta)^{(1+\beta)} \quad (5)$$

(α is obtained from the intercept of the log-log plot; $\gamma=P/a_I^{2/(1+\beta)}$ where a_I is the initial crack length)

The ratio of the crack length a_c and the initial crack length, a_I can be obtained by the initial crack length a_I from the following equation:

$$a_c/a_I=[4/(1-2m)]^{2/(3+2m)} \quad (6)$$

Table 3 gives the values of, k, and, m, of the two FGMs and the monolithic Al_2O_3. **Figure 5** shows their R-curves. The FGMs exhibited steep R-curves with the residual compressive stress in the outer layers, that can lead to higher crack growth resistance and damage tolerance.

Figure 6 shows an optical microscope photo of a notched sample. Referring to the standard method for measuring plane-strain fracture toughness of metallic materials, ASTM E-399, the apparent fracture toughness of the grade materials was calculated from following formula:

$$K_{IC}^a=P_fSY(\alpha)/BW^{1/2} \quad (7)$$

where P_f is fracture load, S is span, B is the specimen thickness, α=a/W (a is the notch length and $Y(\alpha)$ is a nondimensional stress-intensity coefficient given by the following equation:

$$Y(\alpha)=3\alpha^{1/2}[1.99-\alpha(1-\alpha)(2.15-3.93\alpha+2.7\alpha^2)]/2(1+2\alpha)(1-\alpha)^{3/2} \quad (8)$$

Figure 7 gives the apparent fracture toughness of the Al_2O_3-10v.%SiC FGM as a function of the notch depth. The toughness increases with the growth of notch depth in the compressive stress zone and is higher than that of the monolithic materials with compositions of the outer layer (4~5MPam$^{1/2}$) and the intermediate layer (7.2MPam$^{1/2}$). In the tensile area, the value decreases gradually. At the interface of tension and compression, the apparent fracture toughness reaches its maximum 33MPam$^{1/2}$. J. Lin and Y.Miyamoto[7] calculated the stress distribution at the tip of a notch in the compression area of the Al_2O_3/TiC/Ni FGM by FEM. The result shows that the compression stress is over 1GPa around the tip of a notch due to the stress concentration. It is considered, therefore, that such high concentration of compressive stress at the crack tip effectively suppresses the crack initiation and extension from the notch root.

Table 3 The values of k and m.

Materials	k	m
Monolithic Al_2O_3	11.9	0.112
Al_2O_3 FGM	40.4	0.195
Al_2O_3-10v.%SiC FGM	80.5	0.252
Al_2O_3-15v.%SiC FGM	125.6	0.288

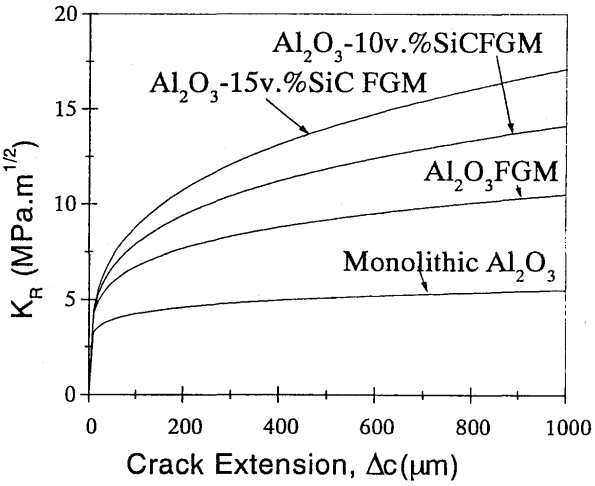

Fig. 5 R-curves of Al_2O_3-SiC FGMs and monolithic Al_2O_3.

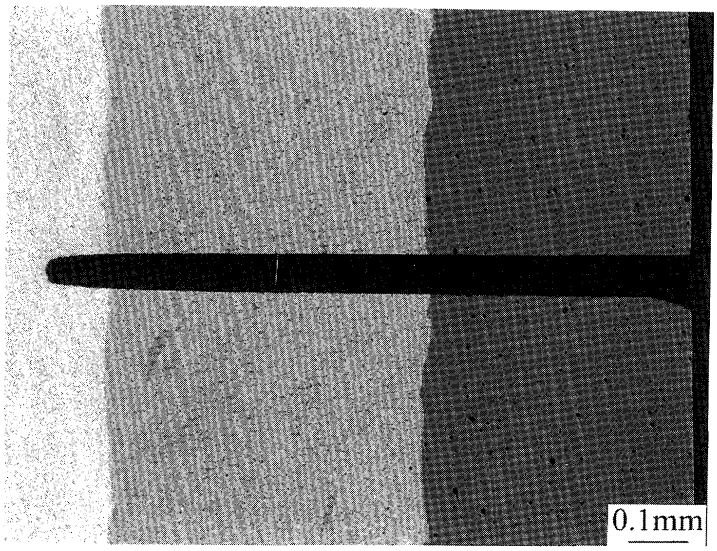

Fig. 6 An optical image of a notched specimen (Al_2O_3-10v.%SiC FGM).

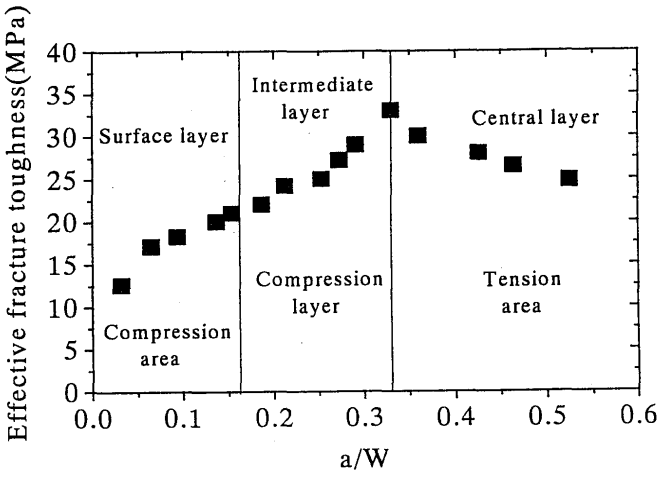

Fig. 7 Effective fracture toughness of the Al_2O_3-10v.%SiC FGM as a function of the notch depth.

4. Conclusions

A dense Al_2O_3-SiC/TiC/Ni FGM was fabricated by SHS/HIP. Because of the compressive residual stress created in the outer ceramic layers and induced by the thermal expansion mismatch of the inner and outer layers, the outer ceramic layers were strongly toughened. The compressive residual stress in the surface leads to steep R-curve behavior of FGMs and significantly enhanced crack growth resistance and damage tolerance.

When the notch depth increases in the compressive stress area due to the stress concentration at the root of notch, the apparent fracture toughness evaluated by the SENB method increases sharply and reaches its maximum 33MPam$^{1/2}$ at the interface of compression and tension fields. Once the notch enters the tension area, the toughness value begins to decrease.

References

1) J. Selsing, "Internal Stresses in Ceramics", J. Am. Ceram. Soc., 44 [8] 419 (1961).
2) R. A. Culter, J. D. Bright A. V. Virkar and D. K. Shetty, "Strength Improvement in Transformation Toughened Alumina by Selective Phase Transformation", J. Am. Ceram. Soc., 70 [10] 714-18 (1987).
3) L.-Y Chao, R. Lakshminarayanan, D K Shetty, and R. A. Culter, "Rolling Contact Fatigue and Wear of CVD- SiC with Residueal Surface Compression", J. Am. Ceram. Soc., 87[9] 2307-13 (1995).
4) H. P. Kirchner, Strengthening of Ceramics, Treatments, Tests and Design Application. Marcel Dekker, New York, 1979.
5) D. J. Green, "A Technique for Introducing Surface Compression into Zirconia Ceramics", J. Am. Ceram. Soc., 66[9] C-178-C-179 (1983).
6) A.G. Merzhanov, "Advanced SHS Ceramics: Today and Tomorrow Morning", Pro. Centennical Int. Symp., The Ceram. Soc. Japan. P. 395 (1991).
7) J. S. Lin and Y. Miyamoto, " Notch Effect of Surface Compression and Toughening of Graded Al_2O_3/TiC/Ni Materials", Acta mater. 48 (2000) 767-775.
8) H. Moriguchi and A. Ikegaya, "Cutting Performance of Hyperfunctional Ceramics", Powder & Powder Metall. 42 [12] 1389-1393 (1995) (in Japanese).
9) Y. Miyamoto, K. Tanihata, T.Kawai and K.Nishida, "Gas-Pressure Combustion Sintering (SHS/HIP) using Silicon Fuel", Pro. In. Conf. On Hot Isostatic Pressing' 93, Elsevier, P. 275, 1994.
10) K. Niihara, R. Morena and D. P. H. Hasselman, " Comment on Elastic/Plastic Indentation Damage in Ceramics: The Median/Radial Crack System", J. Am. Ceram. Soc., 65, C-116 (1982).
11) R.F. Krause, "Rising Fracture Toughness from the Bending Strength of Indented Alumina Beams", J. Am. Ceram. Soc., 71 [5] 338-43 (1988).
12) Y. W. Kim and M. Mitomo, "R-curve Behaviour of Sintered Silicon Nitride", J. Mater. Sci., 30 (1995) 4043-4045.
13) In ASTM E-399-83, Annual Book of ASTM Standards, Section 3, American Society for Testing and Materials, Philadelphia, PA, 1984.
14) D. B. Marshall and B. R. lawn, "An Indentation Technique for Measuring Stress in Tempered Glass Surface", J. Am. Ceram. Soc., 60, P.86 (1977).
15) R. Lakshminarayanan, D. K. Shetty and R. A. Cutler, "Toughening of Layered Ceramic Composites with Residual Surface Compression", J. Am. Ceram. Soc. 79 [1] 29-87 (1996).